RSC Publishing Faraday Discussions

The influence of aqueous solvent on the electronic structure and non-adiabatic dynamics of indole explored by liquid-jet photoelectron spectroscopy

Journal:	*Faraday Discussions*
Manuscript ID	FD-ART-06-2018-000123
Article Type:	Paper
Date Submitted by the Author:	15-Jun-2018
Complete List of Authors:	Kumar, Gaurav; University of Southern California, Department of Chemistry Roy, Anirban; University of Southern California Dana and David Dornsife College of Letters Arts and Sciences, Chemistry McMullen, Ryan; University of Southern California Dana and David Dornsife College of Letters Arts and Sciences Kutagulla, Shanmukh; University of Southern California Dana and David Dornsife College of Letters Arts and Sciences, Chemistry Bradforth, Stephen; University of Southern California, Department of Chemistry

The influence of aqueous solvent on the electronic structure and non-adiabatic dynamics of indole explored by liquid-jet photoelectron spectroscopy

Gaurav Kumar, Anirban Roy, Ryan S. McMullen, Shanmukh Kutagulla and Stephen E. Bradforth*

Department of Chemistry, University of Southern California, Los Angeles, CA 90089, USA

Figures: 9

Tables: 2

* stephen.bradforth@usc.edu, Tel: (213) 740-0461. Fax: (213) 740-397

Abstract

Understanding how the electronic structure of an aqueous solute is intricately bound up with the arrangement of a host liquid provides insight into how non-adiabatic photochemistry takes place in the condensed phase. For example, the presence of water provides additional solute-solvent interactions compared to non-polar solvents: changing the stability of ionized products, modifying the energies of low-lying excited valence states as well as moving the point of intersection between potential surfaces. Thus, the locations and topology of conical intersections between these surfaces also change. The overall impact of the aqueous environment can be to modify the intricate photochemical and non-radiative pathways taking place after photoexcitation. Time-resolved photoelectron spectroscopy (TRPES) in a liquid microjet is here implemented to investigate the influence of water on the electronic structure and dynamics of indole, the chromophore of the amino acid tryptophan. TRPES is used to establish ultrafast relaxation pathways that vary as a function of excitation wavelength. In our experiment, aqueous indole was excited with femtosecond pulses centered at 292 nm and 266 nm. The vertical excitation energy (VIE) of aqueous indole is extracted and found to be lowered by 0.5 eV in water relative to the gas phase. In the TRPES study, the spectral signature of ^1L_a and evidence of solvated electron formation on an ultrafast timescale are observed. Our data also points to a possible contribution of the dissociative $\pi\sigma^*$ state, which can be accessed by a conical intersection (CI) with the ^1L_a state.

I. Introduction

The complex yet fundamental photophysics and photochemistry of tryptophan, one of the essential amino acids, is of considerable importance due to its pivotal role in numerous biological processes/pathways.[1-4] Tryptophan absorbs strongly in the ultraviolet region of the solar spectrum. The absorption and emission bands for tryptophan are well separated and its fluorescence emission is highly sensitive to its local environment which makes it a good probe to study the dynamics of proteins in different environments.[5, 6] In addition to being an important intrinsic probe for studying protein dynamics, it also provides a spectroscopic handle for the determination of the presence of amino acids in astrobiological studies.[7-9]

The photophysics of tryptophan is governed by its chromophore indole. Because of the importance of the tryptophan residue, there is an extensive spectroscopic literature on indole ranging from high-resolution molecular-beam electronic spectroscopy to sub-picosecond ultrafast spectroscopy in a variety of solvents, including water.[10-16] The fluorescence decay of indole in water shows a mono-exponential decrease fluorescence decay with a 4.3 ns lifetime, while in contrast aqueous tryptophan is described by a double exponential decay with lifetimes of 3.14 ns and 0.51 ns. The additional complexity for tryptophan results from the multiple rotamers existing at room temperature with different deployment of the charged amino acid elements attached to the indole chromophore.[17, 18] The single fluorescence lifetime for indole belies the fact that considerable picosecond and sub-picosecond dynamics have been implicated for the excited state chromophore in water, including a significant fraction of the excited state population branching into a photoionization channel to generate solvated electrons.

It is the presence of close-lying electronically excited states in the UV-absorbing amino acids and their molecular precursors (indole for tryptophan; phenol for tyrosine) that vastly increase the complexity of their excited state dynamics.[19-22] In order to understand the fast electronic and nuclear dynamics, uncovering the time-evolving electronic character of the excited state has turned out to be very important. The Born-Oppenheimer approximation breaks down as two potential energy surfaces, belonging to different electronic states, approach each other.[23] In other words, the coupling between the electronic and nuclear degrees of freedoms results in nonadiabatic pathways for electronic relaxation.

Non-adiabatic dynamics is often manifested at conical intersections where two potential energy surfaces would otherwise cross. In indole, the absorption spectrum is dominated by two bound $^1\pi\pi^*$ valence states, known as the ^1L_a and ^1L_b (in accordance with Platt-Murrell nomenclature[24, 25]), which cross a dissociative surface with $\pi\sigma^*$ character along the N-H coordinate. The $\pi\sigma^*$ state also exhibits a conical intersection (CI) with the ground electronic state at elongated N-H distance. [12, 26-28] Due to presence of multiple conical intersections, the excited state relaxation pathways, even in the isolated molecule, can become quite rich.

According to UV-absorption spectra **(Figure 1)**, excitation in the longest wavelength UV region (which is the focus of most experimental studies including this one) involves the optically accessible low-lying excited states which are of ππ* and πσ* character. The broad peak in the range of 220 - 280 nm is primarily attributed to the absorption from the ground state to the ^1L_a. The other ππ* state, ^1L_b, mainly contributes in the region longer than 280 nm. In water, the maximum of the absorption spectrum shifts towards a longer wavelength by ~20 nm. It has been determined experimentally that the band origin of ^1L_b and ^1L_a lies around 283 nm and 273 nm[29, 30] in the gas phase respectively. Although both ^1L_a and ^1L_b are of ππ* character, their static dipoles are markedly different.[31] In the gas phase, the maximum of ^1L_a absorption always lies above the maximum of ^1L_b which makes ^1L_b the fluorescent state according to Kasha's rule. But dissolved in solvent, the relative energy separation between ^1L_a and ^1L_b in indole strongly depends on the dielectric constant of the medium. Due to the large static dipole (6.12 D) of the ^1L_a state, it is stabilized in polar environments, like water, due to dipole-dipole interactions. This results in the lowering of ^1L_a relative to ^1L_b to an extent where ^1L_a now becomes the state where emission originates and the fluorescence spectrum exhibits a large Stokes shift.[31-33] Figure 1b shows the resolution of the excitation spectrum of indole along with the relative contribution of the ^1L_a and ^1L_b states.[34, 35] There is still a debate in the literature whether the reversal of energy order for ^1L_a and ^1L_b happens before or after excitation. Roos and coworkers have shown computationally that the vertical excitation energy to ^1L_a and ^1L_b changes by 0.06 eV and 0.03 eV, respectively, in water but the vertical Franck Condon (FC) region in the ^1L_a state remains higher in energy than ^1L_b. In other words, the solvent affects mainly the emission properties of indole.[32]

Despite the wealth of literature on gas-phase spectroscopy and electronic structure theory, aqueous phase studies are still not conclusive. Excited state studies of indole and tryptophan

have been carried out using pump-probe spectroscopy and fluorescence upconversion, however a clear unified picture has not emerged.[11, 13] Kohler and coworkers focused on the photoionization dynamics of indole in water ensuing excitation at 260 nm and confirmed the generation of the solvated electron within their experimental time resolution of 200 fs. They also suggested that the geminate recombination between the indole radical cation and the solvated electron appears to be surprisingly slow, taking place only on a near-nanosecond timescale.[10] Chergui and coworkers reported the relaxation dynamics of tryptophan in water using fluorescence up-conversion and concluded that the internal conversion between ^1L_a to ^1L_b occurs in only 45 fs while the solvation dynamics has two characteristic time scales, 160 fs and 1 ps.[13] Haacke and coworkers have also reported a similar time scale for the solvent relaxation.[11] There has been no report implicating the involvement of the $\pi\sigma^*$ state of indole (or tryptophan) in the liquid solution. On the other hand, time-resolved photoelectron spectroscopy (TRPES) of gas-phase indole is strongly suggestive of the involvement of the $\pi\sigma^*$ state at four different excitation wavelengths from 249 nm and 273 nm.[26, 36]

Recently, the labs of Lübcke and Neumark have published a series of papers on aqueous nucleic acid monomers (bases, nucleosides and nucleotides) by using liquid jet implementation of TRPES, with the goal of unraveling the excited state population dynamics by mapping the electronic character of the populated excited state onto the ionization continuum.[37-40] These pioneering experiments suggest the promise, and some limitations, of this technique in studying excited state dynamics of solvated molecules.

In this paper, our goal is to apply TRPES in a liquid micro-jet to elucidate the pathways of electronic relaxation for both aqueous indole and tryptophan. In many ways, the excited state dynamics of the chromophore in these systems are less complex than the nucleobases, which are very short-lived in their electronic excited states. In this study, we emphasize the role that solvent plays in controlling excited state dynamics, as manifested in (*i*) solvent-induced changes to the solute valence electronic structure, (*ii*) the role the solvent plays in stabilizing charge-separated states relative to the gas-phase, and (*iii*) how the presence of solvent molecules modifies the approach to the conical intersections which in turn controls photochemical branching. Through Koopmans' theorem, the principal observable of photoelectron spectroscopy is information about the valence orbitals. The valence orbitals are directly connected with

chemical reactivity and we attempt to read out how these orbitals change along the excited state relaxation pathway within the medium relevant for photobiological function.

II. Experimental

Liquid-jet photoelectron spectrometer: The current experimental set up has been improved from the version described earlier.[41] A dual-piston reciprocating solvent pump designed to eliminate mobile-phase pulsed flow in high pressure liquid chromatography (Shimadzu LC-20AD) is used to inject the aqueous solution through a 25 μm diameter fused silica jet nozzle into a vacuum chamber, forming a jet with a flow velocity of ~20 m/s. The solvent pump is run in constant flow rate mode (0.5 ml min^{-1}) to prevent fluctuations in flow which may bring about signal breathing. A typical pressure supplied by the solvent pump varies between 0.1 - 0.3 Mbar to maintain target flowrate. The vacuum chamber is split into a main chamber and a time of flight tube; both are evacuated by separate turbomolecular pumps. The main vacuum chamber is pumped by a large turbomolecular pump (Hi Pace Turbo 1500; 1500 l/s; Pfeiffer Vacuum) and two liquid nitrogen cooled cryotraps. During liquid jet operation in the main chamber, the traps combined with the turbomolecular pump achieve an operating pressure of ~$3x10^{-4}$ mbar in a water-based experiment. The time-of-flight (TOF) tube of ~ 50 cm length (diameter 10 cm) is evacuated with two turbomolecular pumps (Hi Pace 300; 300 l/s, Pfieffer) situated at the detector-end of the drift tube.

Photoelectrons are detected and analyzed with a home-built magnetic bottle TOF photoelectron spectrometer, to ensure high electron collection.[42] The permanent magnet in the magnetic bottle configuration is composed of a soft-iron tip (45^o angle) mounted in the center of a cylindrical 1T SmCo magnet in the main chamber (High Magnetic field). The second part of the magnetic bottle consists of a copper solenoid wound around the flight tube, from which a 1 mT magnetic field (Low Magnetic Field) emanates when 3 A of current is passed through the solenoid. The soft-iron tip is secured in the center of the SmCo magnet by an aluminum jacket such that the position does not change between experiments. The SmCo/soft-iron tip assembly is mounted on a PEEK rod and is attached to a load-bearing XYZ manipulator via an edge-welded bellows for alignment purposes **(Figure 2).**

The photoelectrons are generated by the ultrafast DUV pulses at a distance of less than 1 mm from the skimmer in order to minimize inelastic scattering from vapor-phase molecules surrounding the jet. Ejected electrons are channeled to the flight tube through a 400 μm diameter skimmer and detected using a pair of 40 mm diameter microchannel plate (MCP) detectors in a chevron configuration (Beam Imaging Solutions). In all of our experiments, the pressure inside the time-of-flight was maintained at $2x10^{-6}$ mbar using two turbomolecular pumps.

Typically, in photoelectron spectroscopy the electron binding energy is computed from the difference in the photon energy employed and the electron kinetic energies recorded. One important factor, which can lead to potential misinterpretation of the experimental data is the influence of inelastic scattering. Due to scattering before the electron leaves the liquid, the kinetic energy imparted immediately to the electron upon ejection from the parent molecule may be reduced before escape into the vacuum. Consequently, the recorded value at the detector will be correspondingly lowered. The probability of scattering and the average energy loss depends on the initial kinetic energy of the electron. It should be remembered that as the ionizing light is tunable, even the same photo emission (PE) band recorded with different photon energies may change.[43] The electrons ejected through the liquid in the electron kinetic energy (eKE) range of $0.5 < eKE < 3$ eV in liquids are significantly affected by scattering and energy loss, which results in the distortion of the photoelectron spectra and resultant ambiguities in the accurate determination of electron binding energies. Recently, Luckhaus *et al.* carefully examined this issue and reported the contribution of inelastic scattering by comparing the experimental photoelectron spectra ($3.6 \text{ eV} \leq h\nu \leq 13.6 \text{ eV}$) of the same aqueous species with the Monte Carlo simulations that include inelastic scattering.[43] This study finds that electrons with eKE ≈ 0.75 eV are minimally affected by scattering while electrons departing with 1.5 eV eKE are shifted by as much as 0.5 eV. Thus, to fully recover a genuine binding energy spectrum from a measured liquid jet PE spectrum, it would be necessary to simulate the expected photoelectron spectrum from a theoretical parent binding energy spectrum to include the contribution from inelastic electron scattering.

An important parameter of this magnetic bottle spectrometer is the transmission function (or cut-off function) which determines the detection efficiency as a function of electron kinetic energy. Typically, the detection efficiency of a magnetic bottle spectrometer drops at low kinetic energy

from slow electrons not reaching the MCP detector due to stray fields. Although, the actual form of the transmission function (or more crudely the cut-off threshold) is so far undetermined in our experimental set-up, it is expected, based on observed peak shapes from multiple differing experimental target systems, that the transmission drops rapidly below 0.5 eV electron kinetic energy.[44]

In time-resolved configuration, the two laser beams are spatially overlapped on the laminar flow region of the liquid jet. The excitation wavelengths and the pulse energies used in the experiment are chosen carefully to ensure that no three-photon ionization from water occurs. A tunable pump beam (240-350 nm) is generated by doubling the visible output from a homemade Non-collinear Optical Parametric Amplifier (NOPA) following the design of Riedle *et. al*.[45, 46] The NOPA is pumped with the output of a 35-fs Ti:Sapphire amplifier system (Coherent Legend Elite USP, 1 kHz repetition rate). To accomplish optimal temporal resolution in our experimental setup, the visible output and the second harmonic of the NOPA are compressed using prism-pair compressors, with prisms of fused silica and calcium fluoride respectively. The second, probe, beam fixed at 266 nm is generated by sum frequency of the regenerative amplifier fundamental (centered at 800 nm) and its second harmonic in a BBO Type II crystal of 150 μm thickness. To compensate for dispersion in the optics making up the probe beam path, the 266 nm is also compressed using a calcium fluoride prism-pair compressor before directing to the liquid jet interaction region inside the vacuum chamber. For optimal signal, the spot size of both beams was maintained below 80 μm at the interaction point, as determined by a translating knife edge. Typical pulse energies are 15-25 and 3-5 nJ in the pump and probe, respectively. Unless otherwise stated, the polarization of both beams was vertical with respect to the laboratory frame and perpendicular to the time of flight axis. The experiments using perpendicular polarization were also carried out, with no obvious differences in the signal shapes in the temporal or kinetic energy domains.

In a single-color resonant two photon ionization (R2PI) experiment, a single beam of ultrafast pulses is used to photoionize a chromophore bearing molecule. The first photon absorbed excites the molecule to the intermediate excited state, which is on resonance with the pulse energy, and a second photon absorbed under the same pulse envelope subsequently ionizes the molecule. The R2PI experiments were performed using either at 266 nm or at 292 nm. The typical energies

used for 266 nm and 292 nm pulses were 6 nJ and 35 nJ respectively; it was ensured that the electron count rate was < 10 electrons per shot.

Under our experimental conditions, both the pump and the probe beam individually yield photoelectrons due to resonant one-color two-photon ionization.[41] To eliminate the resonant two photon ionization signals from the transient pump-probe signal, a combination of two identical mechanical choppers (Thorlabs), each operating at 250 Hz with $\pi/2$ phase shift, has been exploited. Using this configuration, one can acquire a complete transient photoemission spectrum from 4 consecutive laser shots without worrying about longer time laser intensity drift and $1/f$ noise.

The pump-probe cross-correlation width was around 190 fs (Figure S1). The non-resonant two color (1+1') multiphoton ionization of sodium iodide solution in water (100 mM) was performed in the microjet. At each delay point, the signal from the pump alone and the probe alone, which were invariant in time, were subtracted from the overall pump-probe signal. The FWHM was extracted after plotting the total PE integrated signal as a function of pump-probe delay time.

Sample preparation: Phenol (≥99.5%; Sigma-Aldrich) and L-tryptophan (>99%; Beantown Chemical) were purchased and used without further purification. Indole (99%; Sigma) was purified to remove brown crystals of presumably oligomers of indole. An amount of 40/60 petroleum ether was added to the impure indole and heated to boiling. Pure indole was dissolved in the top, clear layer of petroleum ether, whilst a layer of molten brown impurity was present in the lower layer. Prior to cooling, the top layer was decanted off from the brown mother liquor, recrystallized and dried under reduced pressure. Solutions of purified indole remain colorless if prepared at a pH 7 buffer and turn yellow if not purified and buffered. Solutions of indole were prepared in a buffer consisting of monobasic potassium phosphate and dibasic sodium phosphate. Two types of stock solutions (4 mM) of the purified indole were then prepared, one with 30 mM NaCl to reduce the jet streaming potential caused by electrokinetic charging and the other with 0.5 M KNO_3, where the nitrate ion serves both as a diffusive scavenger for solvated electrons and also as a static quencher for the primary excited state.[47, 48]

III. Results

Our current study aims to explore the time evolution of the photoexcited state of indole and its parent molecule, tryptophan, as the molecule undergoes non-adiabatic electronic and structural relaxation. PE spectroscopy approaches the problem by mapping out the change in the excited state electronic wavefunction (more correctly for an ensemble measurement, the system density) by projecting it on the basis of cationic states.

Resonant two-photon ionization photoelectron spectra: R2PI-PES of aqueous indole have been recorded under conditions of two photon ionization at 266 nm or 292 nm. The R2PI-PES of indole are shown in **Figure 3**; the equivalent spectra of tryptophan recorded on the same day are shown in the Supplemental Information (Fig. S2). Our main purpose for recording the R2PI spectra is to extract the vertical ionization energies (VIE) of aqueous indole and compare it with indole in the gas phase and aqueous tryptophan. These spectra provide a $t = 0$ slice of the overall dynamics. But they also serve to illustrate the complications and limitations with energy resolving the outgoing electrons emerging from a liquid jet, as discussed in the previous section: namely, that inelastic scattering distorts the PE spectrum, and this does not lead to a simple additive shift because of the electron kinetic energy dependence of the energy loss.

A single very broad photoemission band that cannot be represented by a single Gaussian was observed in the R2PI-PES recorded at 266 nm ionization. It can be well fit by two Gaussians centered at 0.8 and 1.5 eV with an onset at high eKE of ~3.1 eV (the latter is only obvious on a logarithmic eKE scale; the experiment has at least three decades of signal sensitivity). The peak spacing is similar to that fitted for the first and second ionization energies in the XPS (X-ray photoelectron spectroscopy) spectrum of tryptophan (see below).[41] On the other hand, a narrower PE band, which can be fit by a single Gaussian centered at 1 eV and an onset of ~2.5 eV, is observed when 292 nm is employed as the ionizing light. The centers of the higher eKE Gaussians are assigned as the (first) vertical ionization energies and are listed in **Table 1.** In the case of 292 nm, the second ionization band appears to be missing; it either falls well under the transmission cut-off of our instrument or is not present in the data.

The comparison of two R2PI spectra indicates the importance of applying a correction for inelastic scattering to the peaks. According to the simulations of Luckhaus *et al.,* photoelectrons departing with an eKE of 0.8 eV (the center of the 266nm lower band) should be minimally affected by electron inelastic scattering while those at 1.0 eV (292 nm PE center) or 1.5 eV (the

upper band center at 266 nm) would be expected to be affected more significantly.[43] After applying an inelastic scattering correction inferred from ref. [43], the bands at 0.8, 1.0 and 1.5 eV are shifted to the right (towards higher eKE) by 0.05, 0.1 eV and 0.4 eV, respectively. (See S.I. for approximate inelastic energy loss shifts). The computed difference in the corrected eKE between the higher eKE peaks obtained at 266 nm and 292 nm respectively now comes to 0.8 eV; essentially equal to the difference of the doubled photon energy (9.3 eV – 8.5 eV).

Recently, our group reported the vertical ionization energies (VIE) of aqueous tryptophan corresponding to D_0-S_0 and D_1-S_0 with one-photon non-resonant ionization using soft X-rays. We reported 7.3 ± 0.1 eV and 8 ± 0.1 eV using XUV synchrotron radiation at BESSY II.[41] The ionization energies corresponding to D_0-S_0 and D_1-S_0 for indole in water are 7.4 ± 0.1 eV and 8.4 ± 0.1 eV after correction for inelastic scattering for the low eKEs in the R2PI experiments, quite similar to the values reported for tryptophan. As expected, on introducing a condensed polarizable medium, there is a significant decrease in VIE compared to the isolated molecule in vacuum (0.5 eV). The VIE is influenced by the relative stabilization in water of the neutral ground state and the final cationic state (but at the neutral solvent shell structure); the fast electronic polarization of the environment also plays a role.[41, 49] Fielding and coworkers performed R2PI measurements on aqueous phenol as a function of pump wavelength and reported that the D_0-S_0 ionization is lowered by 0.8 eV,[50] which in good agreement with previous XPS measurements reported by Ghosh *et al*.[50, 51] Upon further examination of Table 1, it is evident that hydration has a large effect on the ionization corresponding to D_0-S_0. However, a corresponding increase in the D_1-D_0 gap, at the neutral indole configuration, keeps the D_1-S_0 second ionization energy almost unaltered. A similar effect is observed for tryptophan (see S.I.).

For an R2PI process, the initial excitation to the resonant state and the subsequent ionization take place within the same optical pulse envelope. The ionization rate by the second photon is intensity-dependent and kinetically competes with electronic and nuclear relaxation from the initially excited state. Therefore, the observed vertical ionization energy (VIE) as well as the ionization onset/threshold (AIE) may manifest pulse-width-dependent (and intensity-dependent) character if the relaxation is fast compared to the pulse envelope.[52, 53] From the similarity in the onsets of the R2PI-PES and XPS photoelectron spectra of tryptophan, we previously concluded that the extent of relaxation from solvation and/or intramolecular vibrational

redistribution/vibrational energy relaxation is relatively small for the indole moiety. A time-resolved study can test this notion.

Time-resolved photoelectron spectra: In time-resolved photoelectron measurement, the excitation wavelengths were chosen such that the total photon energy (8.9 eV) is considerably greater than the VIE to the lowest cation state, D_0. Depending on how severe the spectrometer cut-off function is, the cation D_1 is also within reach. With an excitation pulse of 292 nm, the two singlet excited states (^1L_a and ^1L_b) are approximately equally populated as judged by the ratio of absorption strength (^1L_a /^1L_b) at this wavelength.[13, 34] A contour plot showing the photoelectron spectrum as a function of pump-probe delay is displayed in **Figure 4(a)** for aqueous indole following 292 nm excitation; 266 nm here is the probe wavelength. From the spectrum, it is quite clear that a long-lived species is present in the region of 0.5 – 1 eV with a peak maximum at 0.75 eV. In addition to the photoemission band at 0.75 eV, a second distinct but broader band is also apparent in the higher kinetic energy range between 1.2 to 2.3 eV. The photoemission intensity in the higher kinetic range also remains to the longest delays but with less intensity comparatively.

Figure 4(b) represents a contour plot when reversing the pump and probe in terms of the order they intersect the liquid jet. With this ordering, the dynamics recorded reflects an excitation wavelength centered at 266 nm, with the later 292 nm pulse now acting as the ionizing probe pulse. From Fig. 1(b), it can be inferred that at 266 nm, the initially excited population now favors the ^1L_a state by about 3:1. The PE spectrum in Fig 4(b) shows a long-lived structure that is weighted toward the lowest kinetic energy range, but the total PE bandwidth is smaller; the spectrum does not extend to as high eKE in accordance with the smaller energy in the probe photon.

Figure 5 shows the same information as a set of PE spectra at fixed time delays between pulses but is more revealing as to the detail of the spectral dynamics. With 292 nm used for excitation, the PE spectrum shows three time epochs: (i) faster than 500 fs, there is also a developing dip in the PE spectrum around 1.25 eV, (ii) between 1 and 20 ps (Fig. 5(a,b)), it is difficult to see any signal change in the range of 0.5 to 1 eV eKE but the photoemission bands in the higher kinetic range are affected significantly. The colored rectangles illustrate the centers of the three Gaussians which can be used to fit an early time slice. Fig. 5(b) clearly reveals that the higher

eKE photoemission (PE) band which starts centered around 1.8 eV shifts towards lower kinetic energy, converging at around 1.55 eV eKE peak center, with a small decay in overall intensity over 20 ps. There is no accompanying rise anywhere in the spectrum. At longer pump-probe delay (Fig. 5(d)), there is a clear decay of all PE bands but there is no further discernible spectral evolution.

Time slices of the PE spectrum are shown in **Figure 6** when indole is excited instead at 266 nm. It is evident that the spectral shape is completely different compared to 292 nm excitation. A resolved peak at higher eKE is not so evident. In fact, one can observe an isosbestic point (Figure 6(a)) at earliest times which reveals that highest most eKE intensity is decaying while the other PE bands are growing. The spectral feature at lowest eKE appears to be similar to that observed with 292 nm excitation. Because the 4.66 eV excitation photon energy lies above the ionization threshold of indole (4.35 eV) by 0.3 eV,[54] we can expect the generation of solvated electrons to be part of the dynamics. The prompt photoionization yield reported in the literature is 45±15%.[55] Kohler and coworkers have reported the appearance of solvated electrons within 200 fs in aqueous indole with an excitation wavelength of 260 nm. So, a clear possibility for the rise at < 300 fs delay is a contribution of solvated electrons which are expected to overlap in outgoing eKE. As the electrons first trap and then fully solvate, the band will grow first at lower binding energies (high eKE) and then shift from high eKE to lower eKEs, with the lower eKE region expected to grow over the solvation timescale (as observed). Once fully relaxed, we anticipate a binding energy for the solvated electron, $E_b \approx 3.7$ eV,[43] and so an eKE peak center at $h\nu_{probe}$ - 3.7 ~ 0.5 eV (although see below about peak shape).

To verify the signature of the solvated electron, KNO_3 was used as an electron scavenger. Although a strong acid such as HCl is more typically used as a diagnostic solvated electron scavenger, KNO_3 is preferred here over HCl because acidic solutions can initiate the acid catalyzed polymerization of indole.[56] (NO_3^- is also known to act as a scavenger that can quench directly from the optically excited state if the excited state has a spatially extended electronic wavefunction. NO_3^- therefore scavenges the precursors to solvated electrons as well as diffusively scavenging solvated electrons, while H^+ only diffusively scavenges solvated electrons.)[47] From the PE spectra shown in **Figure 7**, we find that the addition of KNO_3 leads to a noticeable increase in the signal decay over the hundreds-of-picosecond timescale for all the PE bands and with a rate commensurate with the known e^-_{aq}/NO_3^- scavenging rate constant and

[NO_3^-] used in the experiment. The impact of scavenging on the PE spectrum is most obvious at the last time slice (300 ps) in Fig. 7(b) where a more structured high eKE peak becomes visible once all the solvated electrons have been scavenged, reminiscent of the 292 nm pump data. Analysis of the quenching experiment is complicated by the fact that nitrate also quenches the excited state directly,[47] a result confirmed by a large quenching of the fluorescence quantum yield in steady state fluorescence measurements on aqueous indole (data not shown).

Polarized pump-probe measurements have also been performed; no anisotropy evolution was observed.

IV. Spectral Analysis

Before attempting to understand the rather subtle time-resolved data for aqueous indole, it is helpful to calibrate expectation and intuition by examining some additional unpublished experimental data for a control system, where we have a clear understanding of what to expect. Aqueous phenol's S_1 excited state is well separated from higher electronic excitations and the excited state dynamics is relatively simple over the first few hundred picoseconds, with very little spectral relaxation observed in water by transient absorption. [20, 21] Therefore, we will attempt to draw a correlation between time-resolved spectra nearby zero pump-probe delay and the R2PI spectrum. Another simplification for aqueous phenol is that the $S_1 \leftarrow S_0$ transition peaks near 266 nm and is non-resonant for the other pulse wavelength used in our experiments, 292 nm. So, for R2PI, two-photons of 266 nm are used to ionize, while for the TRPES, 266 and 292 nm are used for excitation and subsequent ionization, respectively.

In R2PI, the first photon absorbed excites the molecule to the intermediate excited state, and a second photon absorbed under the same pulse envelope subsequently ionizes the molecule. Considering the simplest molecular orbital picture to understand the R2PI spectrum, one would expect the first photon to promote the ring π electron from the HOMO to the LUMO and a subsequent photon to ionize the intermediate excited state to the manifold of cationic states that are connected by one-electron ionization events, i.e., with Koopman's theorem correlations.[57] For a HOMO$\rightarrow$LUMO excitation by the pump, only the D_0 cation state would be expected to have intensity (*i.e,* a single band observed) since the electron configuration of D_0 is best described as a hole in the neutral HOMO. In fact, the 266 nm R2PI spectrum of aqueous phenol

is best described by two Gaussians, separated by a similar spacing (after inelastic scattering correction) to that resolved in the non-resonant XPS spectrum of aqueous phenol and assigned to the D_0 (center eKE = 1.3 eV) and D_1 (center eKE = 0.8 eV) final cation states. This observation can be best explained by configuration interaction in the excited state wavefunction.[41] The amplitude ratio may depend on the relative ionization rate in comparison to the up-pumping rate in the first step as we observe some variation in the peak shape depending on laser conditions.

On the other hand, comparing the 266 nm/292nm PE spectrum obtained at zero pump-probe delay, where the probe photon is less energetic, the PE intensity can be fit by a single Gaussian; (eKE = 0.73 eV center, FWHM ~ 1 eV). We cannot at this point comment on whether a second higher energy PE band is missing or weak, because if present, it would fall under the low eKE cut-off function of our spectrometer. If we compare more carefully the high eKE sides of the R2PI-PES and the 266 nm/292nm PE spectrum obtained at zero pump-probe delay, we might expect that the peaks would be identical in shape but simply at different eKE in accordance with the extra photon energy. From Fig. 8(a), the shape of R2PI and the 266nm/292nm zero-delay spectra indeed are very similar with a shift of 0.4 eV between the peak maxima and the high energy edges. This shift is equal to the difference of the photon energy (4.66 - 4.24 = 0.42 eV) absorbed in the ionization step. This further implies the threshold ionization energies are essentially the same from both spectra.

An important observation is to compare the shape, particularly on the high eKE side of the spectrum for the zero and long inter-pulse delay limits. Molecules excited in the intermediate state have only a finite time to evolve in the excited state before ionization in the zero-delay limit, essentially governed by the pulse length(s) and the intensity-dependent ionization rate. In contrast, in the long delay limit, the excited state molecules can fully relax. Now, if we compare the time-resolved spectrum at the pump-probe delay of 0 and 500 ps (Fig. 8(b)), we observed that the peak maximum is shifted by a minimal amount of 0.08 eV. At 500 ps, we can assign the PE band to originate from ionization of relaxed S_1 and hence the vertical gap corresponding to $D_0 \leftarrow 1^1\pi\pi^*$ is the difference between the probe photon energy and the peak eKE, 4.24 - 0.73 eV = 3.51 eV. It can be seen more clearly from Fig. 8(c) that the S_1 state undergoes very little relaxation over 0.5 ns that impacts the VIE; the VIE changes from 3.43 eV to 3.51 eV, almost within instrumental eKE error. In the case of phenol, most of the excitation energy in excess of the electronic origin goes into perpendicular vibrational modes[58] as ionization is diagonal with

respect to these coordinates. It is understandable that minimal evolution is observed in the aqueous phenol VIE even if vibrational relaxation takes place.

Our analysis of the simple R2PI and time-resolved PE spectrum of phenol hinged on the fact that there was very little solvation or electronic dynamics occurring in the excited state (these changes would be seen in the photoelectron signature) in line with literature expectations. However, if nuclear wavepacket motion occurs along a coordinate where there is a significant displacement between the excited state and cation surfaces, or solvation dynamics or an electronic state change occurs prior to the ionization pulse, then the peak eKE in an R2PI band cannot be simply assigned as the vertical ionization energy of the intermediate excited state. In fact, the peak eKE obtained would be lower than the expected value resulting in overestimation of VIE. Buchner *et al.* has observed this effect for aqueous adenine.[37] Furthermore, there will be substantial changes in the time-resolved PE spectrum matching the relevant timescales of these dynamics.

Now returning to our results for indole shown in Figures 3 - 5, we note the following. At near zero delay:

(1) The 266 nm R2PI spectra (Fig. 3) has been assigned with two Gaussian component bands underlying the broadened peak, based on assignment of non-resonant XPS valence spectra of tryptophan. We therefore assign the two peaks as ionization originating from the HOMO and HOMO-1 orbitals of aqueous indole (Table 1). Unlike the case of phenol, the two bands aren't necessarily the result of configuration interaction in the intermediate state. That is because two overlapping excitation transitions in indole are resonant at 266 nm; Roos *et al.* have assigned as primarily HOMO→LUMO and antisymmetric admixture of HOMO-1→LUMO and HOMO→LUMO+1 for $^1L_a \leftarrow S_0$ and $^1L_b \leftarrow S_0$, respectively.[32]

(2) Because of the 0.81 eV lower total photon energy, the 292 nm R2PI spectra reports on just one component and as commented in the previous section, the impact of the cut-off/transmission function and the larger differences in inelastic scattering shifts leads to greater distortion between the two spectra and poorer matching of the high eKE sides of the PE band shape compared to the model case of phenol. It should also be recognized that different (and non-trival) relaxation dynamics are taking place within the pulse

duration at the two wavelengths, which can be expected to lead to a more physical change in peak shape.

(3) Unlike aqueous phenol, where the two-color time-resolved spectrum obtained at *t=0* displayed an identical shape and high-energy threshold to the R2PI-PES simply with a shift in eKE accounted for by the probe photon energy difference, there is a significant difference between R2PI-PES and TRPES evident for aqueous indole (see **Fig. S3** in the S.I.**)**. Even after accounting for differences in inelastic scattering, there is an introduction of a clear shoulder at higher eKE in the TRPES spectrum.

If we now consider the 292 nm pump TRPES spectra at the longest pump-probe delays where we expect indole to be relaxed electronically and for solvation to be complete, one might naively expect a single spectral feature present corresponding to ionizing the relaxed ^1L_a state, the state responsible for the fluorescence emission of indole. A quick calculation based on the anticipated energy for relaxed ^1L_a (~3.8 eV above the ground state),[33] the corrected VIE of the ground state (Table 1) and application of Koopman's theorem, would estimate an approximate ionization energy (to D_0 cation) for the relaxed ^1L_a of 3.6 eV. So, with a 4.66 eV probe photon this would give rise to a peak at ~ 0.9 eV (after making a small inelastic correction of 0.1 eV). Therefore, the Koopmans' expected feature is the dominant lower eKE peak at 0.75 eV. However, there is a noticeable shoulder at much higher eKE present to the longest pump-probe delays (even well beyond 20 ps trace shown in Fig. 5). From the lower panel of Fig. 5(d) we observe that the slope of all the decay traces over longer time are similar. These observations suggest that the whole PE band belongs to the same electronic state ^1L_a.

Now considering the assignment of the complete evolution of the 292 nm TRPES dataset, it has been reported that the $^1L_a \rightarrow {}^1L_b$ internal conversion (IC) happens in 45 ± 15 fs.[13] Hence, even though at this pump wavelength the excitation approximately equally populates the ^1L_b state, it would be surprising if a signature for the ^1L_b was discernable in our measurement, since this state-switching is faster than the current instrument temporal resolution. If it were, and the ionization cross sections were approximately equal for the two states, one would expect to see a region of the spectrum rising as well as another region decaying. It is possible that the very fast band sharpening and the development of a dip around 1.2 eV is associated with the state

switching but no equivalent gain of PE intensity is seen anywhere else in the spectral window probed.

The time constants of solvation dynamics on the ^1L_a surface on the other hand for tryptophan in water are 160 fs and 1 ps, which means that the signature of solvent relaxation should be observable.[11, 13] We clearly see shifting to lower eKE in the band around 1.8 eV but with a longer associated time constant of ~ 2 ps and surprisingly no apparent shifting of the lower peak centered at 0.75 eV. We will return to this point later.

At lower eKE we have already commented that the spectral shape is being distorted by the decreasing transmission efficiency at these energies. In figure 5(c), we have constructed a simulated time slice using two Gaussians designed to match the experimental time slice measured at *t=20* ps using an estimated cutoff function. The constructed spectrum is quite similar to the experimental time slice and demonstrates how the spectrometer transmission cutoff function affects the spectral feature appearing lower than 0.6 eV. This will become important in making a cross-comparison of the long time PE spectra recorded with two different probe photon energies (Figure 5 and 6).

Switching now to considering the 266 nm pumped experiments (Figure 6), the major impact on the spectroscopy is the ~ 0.4 eV lower probe photon energy. Although 266 nm excitation excites substantially less population on ^1L_b (Fig. 1(b)), as the state switching is not resolved, this will only change the disposition of excess energy. As already discussed, the other major change is that the pump photon energy exceeds the threshold for the photoionization channel; the appearance of solvated electrons in the time-resolved dataset is confirmed by the changes to the TRPES on adding an electron scavenger (NO_3^-) to the indole solution. Other evidence which strengthens the claim of solvated electron formation comes from 266 nm experiments (not shown) conducted on aqueous tryptophan where there is a much less apparent rise in intensity in the lower eKE region of the spectrum that we have assigned to appearance of solvated electrons. Since, the quantum yield of photoionization is three to four times lower in tryptophan compared to aqueous indole,[59-61] it is consistent that a rising feature would not be as noticeable as observed in aqueous indole.

The final puzzle is in considering the long-time PE spectrum. Taking into account that only signatures for the solvated electron and the ^1L_a should remain, and that the ^1L_a features should be

shifted to ~ 0.4 eV lower eKE, it is hard to understand why the dominant feature again appears at 0.75 eV, the same position recorded with a higher probe photon in Figure 5. Figure 6(c) goes some way to explain this observation. The equivalent two peak representation of the ^1L_a signature is used; the center positions of the Gaussians were shifted based on the photon energy used in the ionization step and the contribution coming from inelastic scattering. We also incorporated a third Gaussian here which represents the PE band of solvated electrons. The photoelectron kinetic energy position and FWHM of solvated electron PE band is taken from the ref. 43 and with area consistent with the literature solvated electron yield (assuming equivalent photoionization cross section for e^-_{aq} and ^1L_a). The shape of the constructed time slice (fig. 6(c)) matches qualitatively with the experimental time slice and clearly shows that this experimental spectra is severely affected by the transmission cut-off function of the spectrometer resulting into spectral distortion.

The peak positions of all features in the Figure 5 and 6 are given in Table 2.

V. Discussion

To understand the non-adiabatic dynamics of indole, several time-resolved studies have been performed. Most of the experimental studies focus on the gas phase behavior of this molecule and only a few of them consider the influence of water on the non-adiabatic behavior.[10, 11, 13]

Townsend and his coworkers investigated the spectroscopic behavior of gas phase indole at four excitation wavelengths between 249 nm and 273 nm with the same ionization wavelength of 300 nm using time resolved photoelectron spectroscopy. They concluded that at all wavelengths, the ^1L_a state decays by branching within 100 fs to ^1L_b and to $\pi\sigma^*$; the latter population decays on the order of picosecond residing on the $\pi\sigma^*$ for a surprisingly long time at long R(N-H).[26] The shape and the position of the spectral features were found to be identical for all pump wavelengths. The only difference was the relative amplitude of the features associated with the decay constants of the electronic states, excited directly or indirectly. It was interesting that these authors found two parallel relaxation pathways at all excitation energies. The decay constant associated with $\pi\sigma^*$ decreases slowly and monotonically from 1.2 ps at 273 nm excitation to 0.7 ps at 249 nm excitation. This difference of $\pi\sigma^*$ lifetime may be due to the excess of excitation energy at 249 nm which launches the wavepacket above the 0.45 eV barrier calculated to lie along the N-H

coordinate outside the FC region. An interesting outcome of the experiments from Townsend's group was the apparent involvement of $\pi\sigma^*$ even at the longest excitation wavelength 273 nm.[26]

In the aqueous phase, the landscape of the excited state potential energy surfaces is influenced by the presence of the solvent, which can change the position of conical intersections that drive efficient radiation-less transitions. Several computational studies performed on indole in water reveal that the polar nature of water mainly affects the emission properties of indole leading to inversion of the energy order of ^1L_a and ^1L_b; ^1L_a becomes the emitting state in water.[31, 32, 62] The inversion of the solvent-relaxed electronic states can be explained based on the argument of the higher permanent dipole moment of ^1L_a state; the ^1L_a state becomes lower in energy due to enhanced dipole-dipole interaction in water.[32] Although the relaxed state ordering is inverted compared to the gas phase, the state ordering is unchanged at the level of the vertical excitation energy from the ground state of indole.[32 33] What has not been as well established is the energy of $\pi\sigma^*$. The $\pi\sigma^*$ state has the highest permanent dipole moment (12.4 D) which is almost double than the static dipole of the ^1L_a state (6.2 D), but it also has Rydberg character which can push its energy up in the order due to Pauli repulsion.[26]

In this work, we are interested to see if we can capture the involvement of $\pi\sigma^*$ in the relaxation dynamics of indole in water using TRPES. If we were to follow the proposal by Domcke and coworkers,[62] the fact that solvated electrons are produced with high quantum yields[63] immediately implicates this pathway and we should be looking to connect the spectral signatures of the $\pi\sigma^*$ as it evolves into a solvated electron. Fig. 1(a) reveals that the indole absorption maximum is red-shifted by almost 20 nm in water. Therefore, the experiments here at 292 nm are the closest analogue to the long wavelength excitation experiments in the gas phase, 273 nm, where the $\pi\sigma^*$ is assigned to have its longest lifetime, ~ 1.2 ps. Based on our analysis so far, it is tempting to assign the very highest eKE feature to the πσ* channel. This may be reasonable, as this timescale does not match well with the ^1L_a solvation timescales in water[13] and as commented earlier we see no band shifting for the low eKE feature also assigned to PE signature from the ^1L_a. At 292 nm, we do see a loss of integrated signal with a timescale of 10 ps, and a narrowing of the higher energy side of the 1.8 eV peak without evidence of a rise anywhere else in the PE spectrum.

According to Bernas *et al.,* there should be no solvated electron production as the ionization threshold of indole has been estimated at 4.35 eV using the photoconductivity measurements, which is higher than the excitation energy 4.24 eV (292 nm).[54] Contradicting this observation, Ryuzi Katoh[59] performed nanosecond time resolved transient absorption on aqueous indole to examine the photoionization yield as a function of excitation wavelength (220-290 nm) and concluded that the solvated electrons are produced through a monophotonic process over the entire wavelength range. The long-time quantum yield remained approximately constant at 0.2 for all wavelengths longer than 250 nm. We are unable to observe any concomitant rise in any other PE bands at 292 nm excitation that might be assignable to the solvated electron, unlike at 266 nm excitation. One possibility is the electron being produced on a much slower timescale (but with similar yield to satisfy the hundreds of nanoseconds data of Katoh) and concomitantly with the slow decay of the ^1L_a state, similarly to the case of aqueous phenol at 266 nm excitation.[20]

VI. Conclusion and Outlook

The vertical ionization energies of indole (7.4 ± 0.1 eV, 8.4 ± 0.1 eV) have been measured in water. The presence of aqueous environment lowers the first VIE by 0.5 eV. In our TRPES measurements, we observed clear spectral signatures that can be assigned to ^1L_a state and, with a 266 nm pump, solvated electrons.

With 292 nm excitation, evidence for relaxation within the ^1L_a state is observable in the PE spectrum shifting to lower eKE, however, such dynamics is captured only in one of the two peaks that make up the fingerprint of the ^1L_a state. We speculate that rather than reflecting solvation dynamics, the highest eKE features and their disappearance may be connected with passage via the $\pi\sigma^*$ state of a small portion of the overall excited state population. The picosecond disappearance of this high eKE signal (and the overall PE intensity) corresponds to dissociation (to H atoms) over a $\pi\sigma^*$ barrier without the obvious production of solvated electrons, at least within the hundreds of picosecond delay window of the current experiment. Alternatively, this pathway provides efficient return to the ground state.

Results for a 266 nm pump are consistent also with branching of the population but now on a femtosecond timescale from the initially excited (or rapidly populated) ^1L_a state. Part of the ^1L_a

state population relaxes and decays on the nanosecond time scale via internal conversion while a smaller portion undergoes ultrafast photoionization within 200 fs.[10] Making a connection to the $\pi\sigma^*$ pathway (where there is more evidence in the 292 nm dataset), it is possible that with the higher energy excitation, there is simply no energy barrier on the $\pi\sigma^*$ intermediate state and the larger resulting H-atom translational energy results in water ionization to generate solvated electrons.[62, 64]

In future work, we will follow up by probing for the signature of solvated electrons with electronic transient absorption and their appearance time at 292 nm out to nanosecond time delays. To reinforce the argument for an excitation energy dependent solvated electron generation, solvents that yield higher threshold energies for indole photoionization, (*e.g.,* ethanol) will be tested; we expect features such as the early time rise in the excited state dynamics to be absent. In TRPES, a higher probe energy will be employed in future experiments to avoid the spectrometer cut-off function and fully resolve the ^1L_a signature and solvated electron signatures. A careful choice of probe/ionization photon energy is also necessary to access the complete manifold of FC window, as the molecular system evolves in the excited state.[40] If the probe photon energy would be insufficient to access the FC window for photoionization then the measured lifetime would be less than the actual value as pointed out by Martinez and co-workers.[65]

VII. Conflicts of interest

There are no conflicts of interest to declare.

VIII. Acknowledgements

The assistance of Bastian Baudisch and Professor Eberhard Riedle is gratefully acknowledged in the design of the 35-fs pumped NOPA. We acknowledge support from the National Science Foundation (CHE-1301465) for this project. The authors thank Mike Kellogg for assistance in performing the current experiments and to Seth Wieman of the USC Dornsife/Viterbi machine shop for help in designing and manufacturing improvements to our vacuum chamber.

IX. References

1. S. K. Pal, J. Peon and A. H. Zewail, *Proc. Natl. Acad. Sci.*, 2002, **99**, 1763-1768.
2. S. Schenkl, F. Van Mourik, G. Van der Zwan, S. Haacke and M. Chergui, *Science*, 2005, **309**, 917-920.
3. B. L. Vallee and J. F. Riordan, *Annu. Rev. Biochem.*, 1969, **38**, 733-794.
4. K. S. Sarkisyan, I. V. Yampolsky, K. M. Solntsev, S. A. Lukyanov, K. A. Lukyanov and A. S. Mishin, *Sci. Rep.*, 2012, **2**, 608.
5. P. R. Callis, *Methods Enzymol.*, 1997, **278**, 113-150.
6. J. Lakowicz, *Principles of fluorescence spectroscopy. Kluwer Academic Press,* New York, 1999
7. E. Eshelman, M. Daly, G. Slater and E. Cloutis, *Planet. Space Sci.*, 2015, **119**, 200-207.
8. L. R. Dartnell, T. A. Roberts, G. Moore, J. M. Ward and J.-P. Muller, *PLoS One*, 2013, **8**, 75270.
9. F. Scappini, M. Capobianco, F. Casadei, R. Zamboni and P. Giorgianni, *Int. J. Astrobiol.*, 2007, **6**, 281-289.
10. J. Peon, G. C. Hess, J.-M. L. Pecourt, T. Yuzawa and B. Kohler, *J. Phys. Chem. A*, 1999, **103**, 2460-2466.
11. D. Sharma, J. Léonard and S. Haacke, *Chem. Phys. Lett.*, 2010, **489**, 99-102.
12. R. Montero, Á. P. Conde, V. Ovejas, F. Castaño and A. Longarte, *J. Phys. Chem. A*, 2011, **116**, 2698-2703.
13. O. Bram, A. A. Oskouei, A. Tortschanoff, F. van Mourik, M. Madrid, J. Echave, A. Cannizzo and M. Chergui, *J. Phys. Chem. A*, 2010, **114**, 9034-9042.
14. E. Gudgin, R. Lopez-Delgado and W. R. Ware, *J. Phys. Chem.*, 1983, **87**, 1559-1565.
15. M. R. Eftink, J. Jia, D. Hu and C. A. Ghiron, *J. Phys. Chem.*, 1995, **99**, 5713-5723.
16. J. W. Petrich, M. Chang, D. McDonald and G. Fleming, *J. Am. Chem. Soc.*, 1983, **105**, 3824-3832.
17. N. Periasamy and G. Joshi, *Nuovo Cimento Soc. Ital. Fis., D*, 1990, **12**, 1691-1695.
18. D. Rayner and A. Szabo, *Can. J. Chem.*, 1978, **56**, 743-745.
19. K. Guzow, R. Ganzynkowicz, A. Rzeska, J. Mrozek, M. Szabelski, J. Karolczak, A. Liwo and W. Wiczk, *J. Phys. Chem. B*, 2004, **108**, 3879-3889.
20. T. A. Oliver, Y. Zhang, A. Roy, M. N. Ashfold and S. E. Bradforth, *J. Phys. Chem. Lett.*, 2015, **6**, 4159-4164.
21. Y. Zhang, T. A. Oliver, M. N. Ashfold and S. E. Bradforth, *Faraday Discuss.*, 2012, **157**, 141-163.
22. O. V. Boyarkin, S. R. Mercier, A. Kamariotis and T. R. Rizzo, *J. Am. Chem. Soc.*, 2006, **128**, 2816-2817.
23. M. Born and R. Oppenheimer, *Ann. Phys.*, 1927, **389**, 457-484.

24. J. R. Platt, *J. Chem. Phys.*, 1949, **17**, 484-495.

25. J. N. Murrell, *The Theory of the Electronic Spectra of Organic Molecules,* Chapman and Hall: London, 1971

26. R. Livingstone, O. Schalk, A. E. Boguslavskiy, G. Wu, L. Therese Bergendahl, A. Stolow, M. J. Paterson and D. Townsend, *J. Chem. Phys.*, 2011, **135**, 194307.

27. G. M. Roberts and V. G. Stavros, *Chem. Sci.*, 2014, **5**, 1698-1722.

28. M. G. Nix, A. L. Devine, B. Cronin and M. N. Ashfold, *J. Chem. Phys.*, 2007, **126**, 124312.

29. V. Povedailo and D. Yakovlev, *J. Appl. Spectrosc.*, 2008, **75**, 336-340.

30. B. J. Fender, D. M. Sammeth and P. R. Callis, *Chem. Phys. Lett.*, 1995, **239**, 31-37.

31. A. L. Sobolewski and W. Domcke, *Chem. Phys. Lett.*, 1999, **315**, 293-298.

32. L. Serrano-Andrés and B. O. Roos, *J. Am. Chem. Soc.*, 1996, **118**, 185-195.

33. D. Brisker□Klaiman and A. Dreuw, *ChemPhysChem*, 2015, **16**, 1695-1702.

34. B. Valeur and G. Weber, *Photochem. Photobiol.*, 1977, **25**, 441-444.

35. M. R. Eftink, L. A. Selvidge, P. R. Callis and A. A. Rehms, *J. Phys. Chem.*, 1990, **94**, 3469-3479.

36. M. M. Zawadzki, J. O. Thompson, E. A. Burgess, M. J. Paterson and D. Townsend, *Phys. Chem. Chem. Phys.*, 2015, **17**, 26659-26669.

37. F. Buchner, H.-H. Ritze, J. Lahl and A. Lübcke, *Phys. Chem. Chem. Phys.*, 2013, **15**, 11402-11408.

38. F. Buchner, B. Heggen, H.-H. Ritze, W. Thiel and A. Lübcke, *Phys. Chem. Chem. Phys.*, 2015, **17**, 31978-31987.

39. F. Buchner, A. Nakayama, S. Yamazaki, H.-H. Ritze and A. Lübcke, *J. Am. Chem. Soc.*, 2015, **137**, 2931-2938.

40. H. L. Williams, B. A. Erickson and D. M. Neumark, *J. Chem. Phys.*, 2018, **148**, 194303.

41. A. Roy, R. Seidel, G. Kumar and S. E. Bradforth, *J. Phys. Chem. B*, 2018, **209**.

42. P. Kruit and F. Read, *J. Phys. E*, 1983, **16**, 313.

43. D. Luckhaus, Y.-i. Yamamoto, T. Suzuki and R. Signorell, *Sci. Adv.*, 2017, **3**, e1603224.

44. M. Mucke, M. Förstel, T. Lischke, T. Arion, A. M. Bradshaw and U. Hergenhahn, *Rev. Sci. Instrum.*, 2012, **83**, 063106.

45. S. Lochbrunner, T. Wilhelm, J. Piel, S. Spörlein and E. Riedle, *Adv. Solid State Lasers*, Boston, Massachusetts United States, 1999.

46. E. Riedle, M. Beutter, S. Lochbrunner, J. Piel, S. Schenkl, S. Spörlein and W. Zinth, *Appl. Phys. B*, 2000, **71**, 457-465.

47. X. Chen, D. S. Larsen, S. E. Bradforth and I. H. van Stokkum, *J. Phys. Chem. A*, 2011, **115**, 3807-3819.

48. T. W. Kee, D. H. Son, P. Kambhampati and P. F. Barbara, *J. Phys. Chem. A*, 2001, **105**, 8434-8439.

49. B. Jagoda-Cwiklik, P. Slavíček, L. Cwiklik, D. Nolting, B. Winter and P. Jungwirth, *J. Phys. Chem. A*, 2008, **112**, 3499-3505.

50. J. Riley, B. Wang, J. Woodhouse, M. Assmann, G. A. Worth and H. H. Fielding, *J. Phys. Chem. Lett.*, 2018, **9**, 678-682

51. D. Ghosh, A. Roy, R. Seidel, B. Winter, S. Bradforth and A. I. Krylov, *J. Phys. Chem. B*, 2012, **116**, 7269-7280.

52. G. Mainfray and C. Manus, *Appl. Opt.*, 1980, **19**, 3934-3940.

53. L. Lompre, G. Mainfray and C. Manus, *J. Phys. B: At., Mol. Opt. Phys.*, 1980, **13**, 85.

54. A. Bernas, D. Grand and E. Amouyal, *J. Phys. Chem.*, 1980, **84**, 1259-1262.

55. T. Bizjak, P. Bisht, S. Lochbrunner and E. Riedle, *Femtochem. Femtobiol.*, 2004, 229-232.

56. G. Smith, in *Adv. Heterocycl. Chem.*, 1963, **2**, 287-309.

57. M. J. Vrakking, D. Villeneuve and A. Stolow, *Phys. Rev. A*, 1996, **54**, R37.

58. M. G. Nix, A. L. Devine, B. Cronin, R. N. Dixon and M. N. Ashfold, *J. Chem. Phys.*, 2006, **125**, 133318.

59. R. Katoh, *J. Photochem. Photobiol., A*, 2007, **189**, 211-217.

60. F. Saito, S. Tobita and H. Shizuka, *J. Photochem. Photobiol., A*, 1997, **106**, 119-126.

61. K. L. Stevenson, G. A. Papadantonakis and P. R. LeBreton, *J. Photochem. Photobiol., A*, 2000, **133**, 159-167.

62. A. L. Sobolewski and W. Domcke, *Chem. Phys. Lett.*, 2000, **329**, 130-137.

63. W. G. McGimpsey and H. Görner, *Photochem. Photobiol.*, 1996, **64**, 501-509.

64. C. G. Elles, I. A. Shkrob, R. A. Crowell and S. E. Bradforth, *J. Chem. Phys.*, 2007, **126**, 164503.

65. H. R. Hudock, B. G. Levine, A. L. Thompson, H. Satzger, D. Townsend, N. Gador, S. Ullrich, A. Stolow and T. J. Martinez, *J. Phys. Chem. A*, 2007, **111**, 8500-8508.

66. C. P. Schick, S. D. Carpenter and P. M. Weber, *J. Phys. Chem. A*, 1999, **103**, 10470-10476.

67. J. Eland, *Int. J. Mass Spectrom. Ion Processes*, 1969, **2**, 471-484.

68. L. Dolby, G. Hanson and T. Koenig, *J. Org. Chem.*, 1976, **41**, 3537-3539.

69. L. Domelsmith, L. L. Munchausen and K. Houk, *J. Am. Chem. Soc.*, 1977, **99**, 4311-4321.

70. M. Kubota and T. Kobayashi, *J. Electron. Spectrosc. Relat. Phenom.*, 2003, **128**, 165-178.

Figure 1:

(a) UV absorption spectra of indole in water compared with gas phase and aqueous tryptophan. Two peaks (magenta and blue) represents the wavelength used in our R2PI and TRPES experiments. (b) Deconvolution of the relative contribution of L_a (red) and L_b(blue) from total absorption spectrum of indole in propylene glycol (a hydrogen-bonding solvent) extracted from Ref.[34]

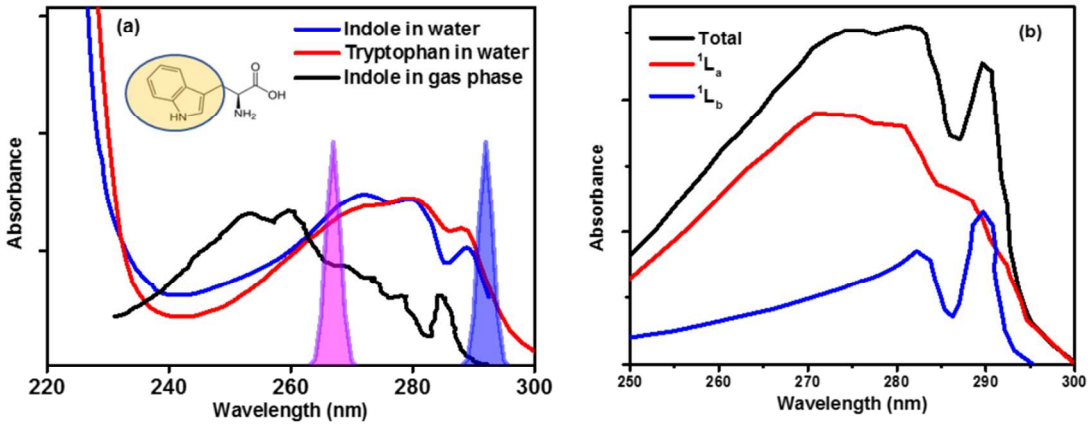

Figure 2:

Experimental design of the liquid-jet time resolved photoelectron spectroscopy apparatus. A jet is formed by forcing the solution of interest through a quartz nozzle (top center) which is ultimately caught by a cryotrap held at liquid nitrogen temperature (bottom center). Both pump and probe are spatially overlapped with each other and with the jet in the laminar region of jet flow. The electron collection efficiency is increased by the use of a magnet assembly (left), which helps guide electrons through the skimmer (right).

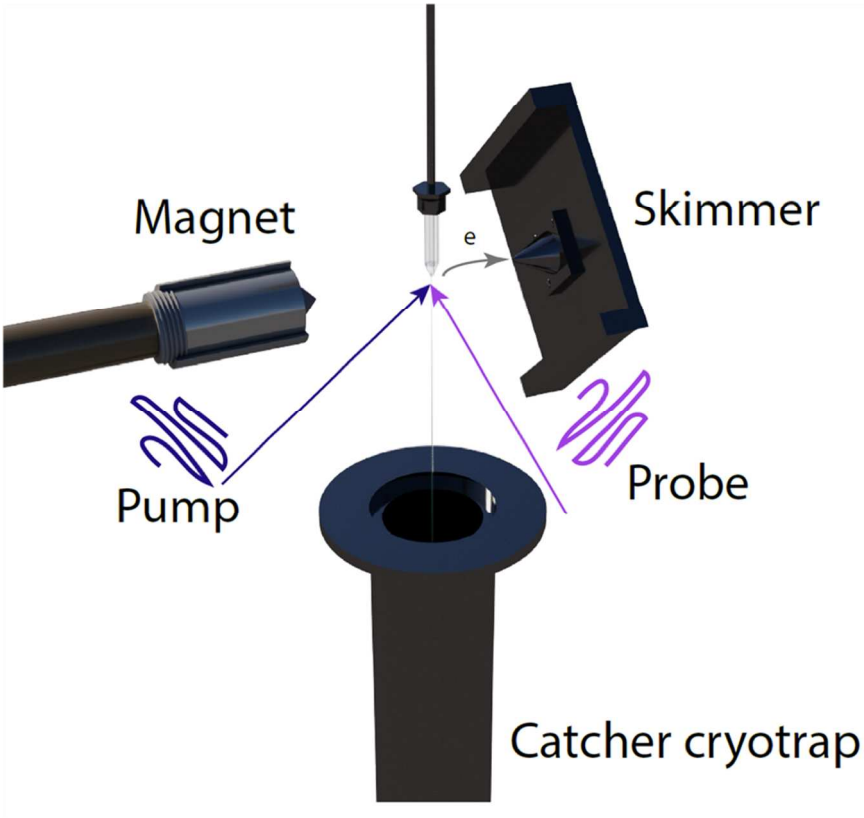

Figure 3:

Resonant two-photon ionization spectra of aqueous indole recorded with a (a) 266 nm ionization and (b) 292 nm ionization wavelength. In panel **(a)** individual Gaussians used to fit the spectrum are shown in red and green; the total Gaussian fit is represented in blue. For panel **(b)** the spectrum can be fit with a single Gaussian (in red). Rectangles depict the center of the Gaussian. Note that the R2PI spectra are affected by instrument transmission function at eKE < 0.5 eV

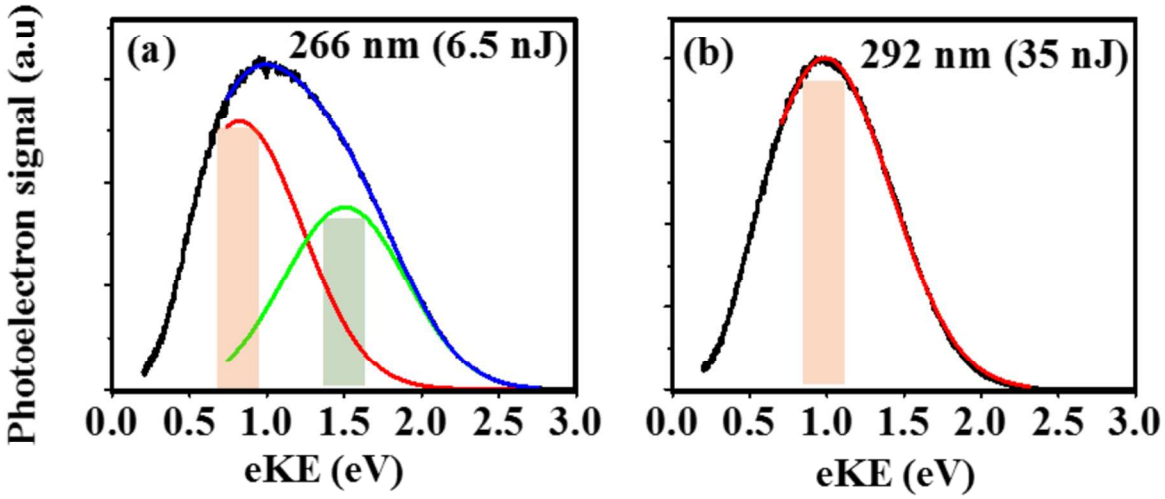

Figure 4:

Time-resolved photoelectron spectra of aqueous indole plotted with pulse time-ordering (a) 292 nm pump with subsequent 266 nm probe and (b) 266 nm pump and subsequent 292 nm probe. Both beams are vertically polarized with respect the laboratory frame.

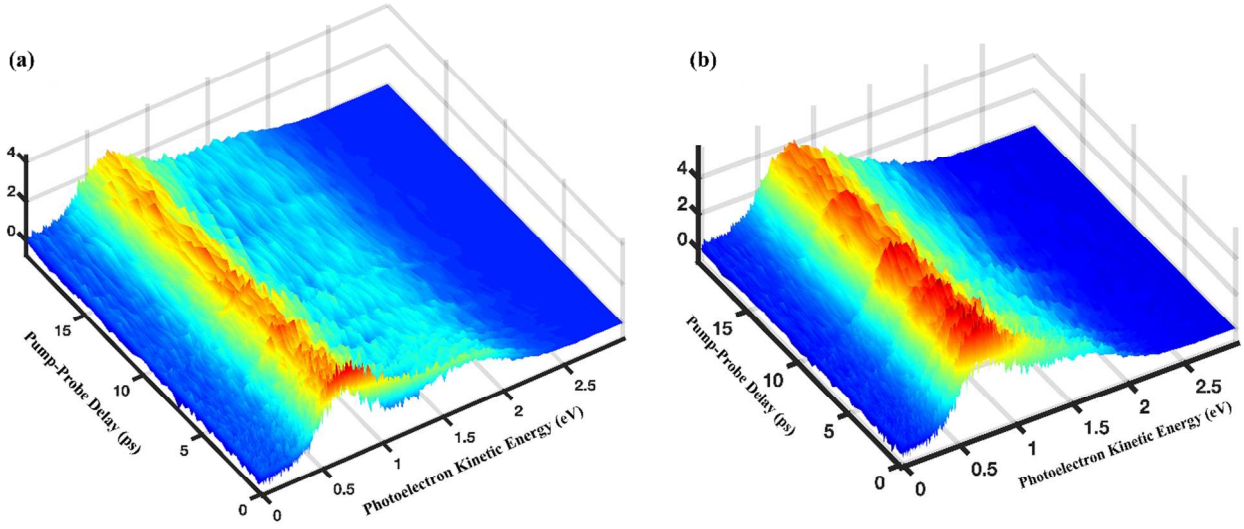

Figure 5:

TRPES spectra extracted from full dataset in Figure 4 (a) where aqueous indole is photoexcited with 292 nm and photoionized with 266 nm subsequently. Panel (a) displays a developing dip around 1.25 eV in the TRPES spectra within half a picosecond while panel (b) mainly demonstrates the shift of higher eKE photoemission bands towards lower eKE with a small decay in overall intensity. Panel (c) displays the comparison between an experimental time slice at 20 ps (orange), for which an attempt to reproduce the spectrum from two Gaussians is also displayed (see text). This does not replicate the experimental slice fully at low electron kinetic energies. But combining these two Gaussians with an estimated cutoff function for our spectrometer now reproduces the rapidly decaying signal intensity at low electron kinetic energies. In panel (d), the PE signal (on logarithmic scale) is plotted at four selected eKEs as a function of time delay. The experimental conditions were different for short time pump-probe delays (upper panel (d)) and for longer delay times (lower panel (d)) measurements (datasets are recorded on different days).

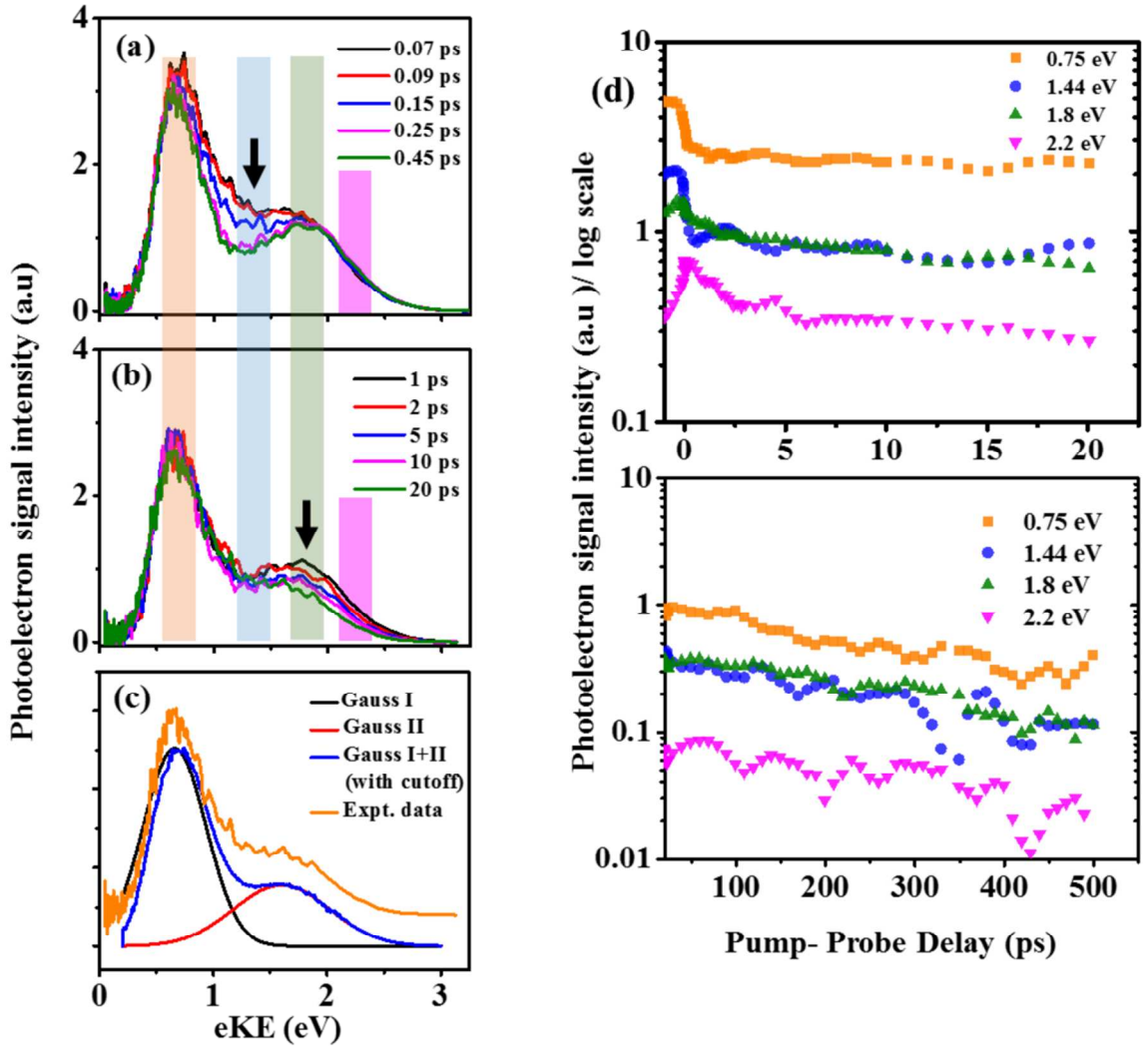

Figure 6:

TRPES spectra extracted from full dataset in Figure 4 (b) where aqueous indole is photoexcited with 266 nm and photoionized with 292 nm subsequently. Panel (a) displays the decay of the highest eKE PE band and the rise of other PE bands—depicted with arrows—resulting into an isosbestic point (at 1.95 eV) within half a picosecond while panel (b) shows a clear decay of the same PE bands over a longer 20 ps timescale. Panel (c) displays the comparison between an experimental time slice (2 ps delay) with a constructed time slice composed of two individual Gaussians belonging to ^1L_a, and a third Gaussian representing the solvated electron along with an estimated cutoff function of the spectrometer (see text for details). In panel (d), the PE signal (on a logarithmic scale) is plotted at four selected eKEs as a function of time delay. Inset of the top panel shows the rising signal in the first 2 ps with a linear signal scale. Experimental conditions were different for short time pump-probe delay (upper panel (d)) and for long time pump-probe delay (lower panel (d)) measurements (datasets recorded on different days). The mutual polarization of the two beams is parallel.

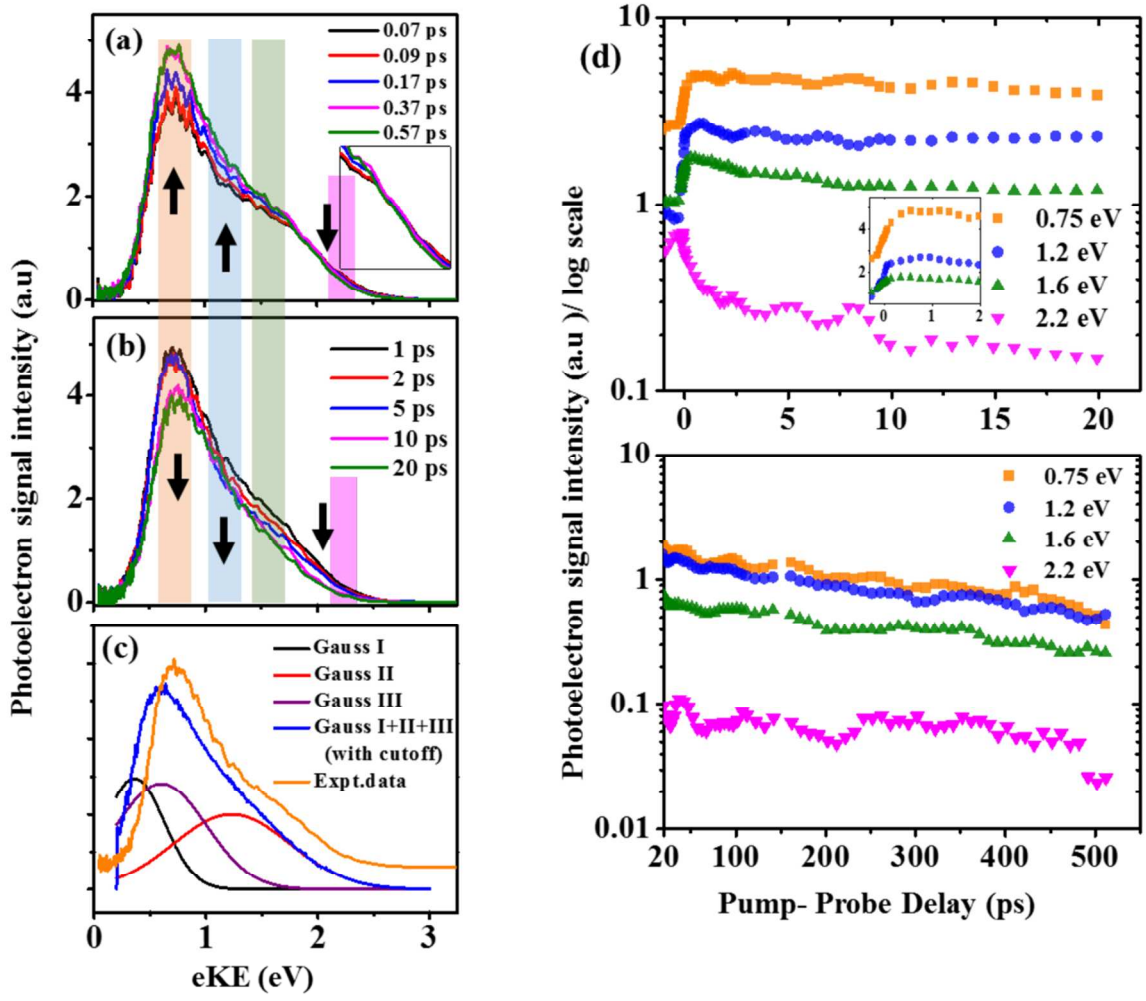

Figure 7:

TRPES spectra at selected pump-probe delay for (a) 4 mM indole in water (b) 4 mM indole with 0.5 M KNO3 (quencher) in water, both measured with 266 nm excitation and 292 nm ionization. The nitrate anion quenches both solvated electrons as well as the excited state, resulting in an increased decay rate of all the PE bands as displayed in panel (c). Note that the signal axis in (c) is plotted on logarithmic scale. The polarization of the pump and probe are perpendicular with respect to each other.

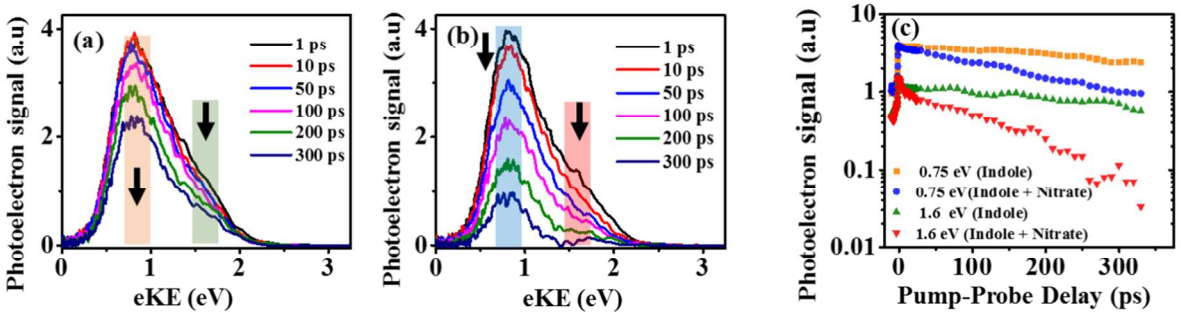

Figure 8:

R2PI spectrum of phenol (20 mM solution; 266 nm ionization pulse) is compared with the TRPES spectrum of phenol when both 266 nm and 292 nm pulses are temporally overlapped i.e. at time zero. Individual Gaussian fits and total fit are shown in magenta, green and blue color respectively for R2PI while red line displays a single Gaussian fit for the TRPES spectrum. Panel (b) displays a small shift in peak maximum (0.08 eV) between the TRPES spectrum of aqueous phenol at *t=0 ps* and *t=500 ps*. Panel (c) shows TRPES spectra of aqueous phenol at different pump-probe delays and illustrates no change in spectral shape. The peak height decay likely reflects imperfect laser spot overlap across the length of the delay stage. The excited state lifetime for aqueous S_1 phenol is 3.4 ns. The polarization of both beams is parallel with respect to each other.

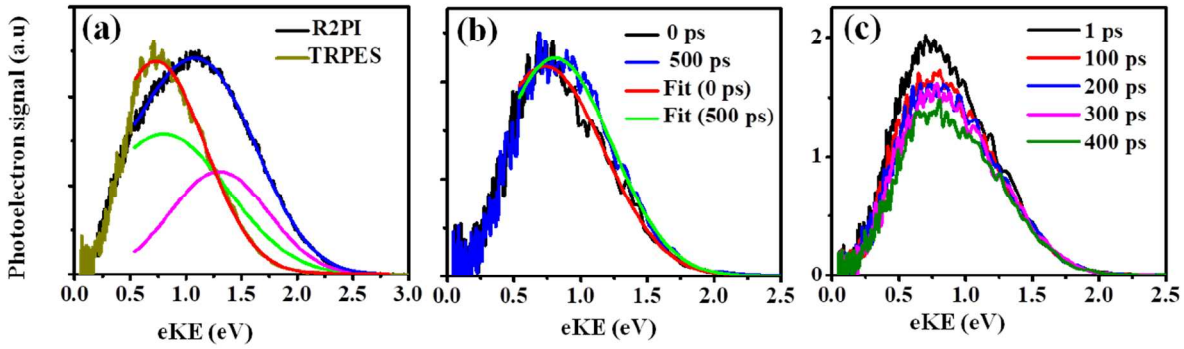

Figure 9:
The presence of two ionization peaks in R2PI-PES experiment emphasizes the contribution of configuration interaction also found in gas phase phenol.[66]

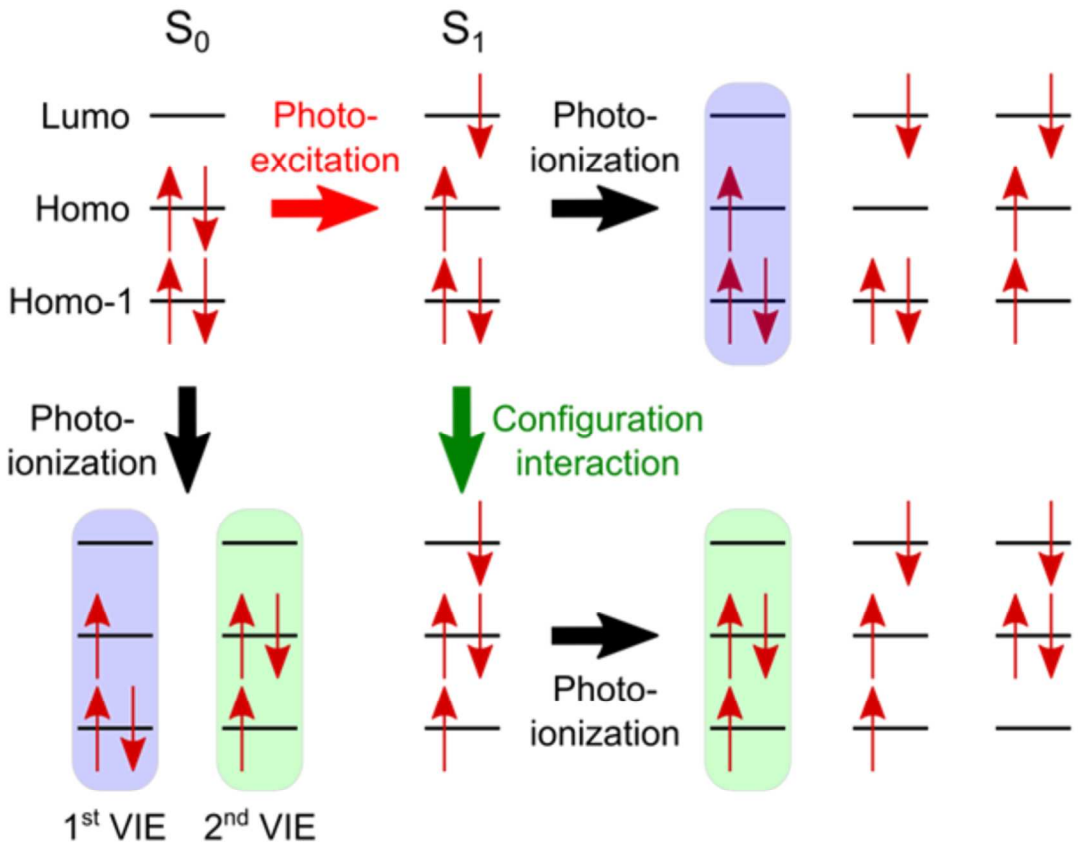

Table 1: **R2PI peak positions and derived vertical ionization energies for aqueous indole compared with the isolated molecule in the gas phase. All energies in eV.**

Ionized orbital	eKE[a] (266 nm R2PI/ 292 nm R2PI)	Corrected eKE[b] (266 nm R2PI/ 292 nm R2PI)	VIE[c] (266 nm R2PI/ 292 nm R2PI)	VIE[d] (gas phase)
HOMO (π_3)	1.5 / 1	1.9 / 1.1	7.4 / 7.4	7.9
HOMO-1(π_2)	0.8 / -	0.9 / -	8.4 / -	8.4

[a] electron kinetic energies

[b] eKE reported after correcting for electron inelastic scattering

[c] vertical ionization energies

[d] VIE reported in gas phase[67-70]

Table 2: Binding energies (BE) extracted from corresponding eKE peaks in TRPES spectrum. All energies in eV.

292 nm pump (excitation) and 266 nm probe (ionization)

PE Bands	eKE	Corrected eKE	BE ($h\nu_{probe}$ - eKE)
PE I[a]	0.75	0.75	3.9
PE II	1.4	1.8	2.9
PE III	1.8	2.3	2.3

266 nm pump (excitation) and 292 nm probe (ionization)

PE Bands	eKE	Corrected eKE	BE ($h\nu_{probe}$ - eKE)
PE I[a]	0.75	0.75	3.5
PE II	1.2	1.5	2.7
PE III	1.6	2	2.2

[a] Peak position strongly affected by spectrometer cut-off function on low eKE side.